

# Dynamic Contrast-Enhanced MRI Parameters as Biomarkers in Assessing Head and Neck Lesions After Chemoradiotherapy Using a Wide-Bore 3 Tesla Scanner

Gergely Lerant<sup>1</sup> · Peter Sarkozy<sup>2</sup> · Zoltan Takacsi-Nagy<sup>3</sup> · Gabor Polony<sup>4</sup> · Laszlo Tamas<sup>4</sup> · Erika Toth<sup>5</sup> · Andras Boer<sup>6</sup> · Laszlo Javor<sup>1</sup> · Maria Godeny<sup>1,7</sup>

Received: 5 September 2014 / Accepted: 21 April 2015 / Published online: 30 April 2015  
© Arányi Lajos Foundation 2015

**Abstract** Pilot studies have shown promising results in characterizing head and neck tumors (HNT) using dynamic contrast-enhanced magnetic resonance imaging (DCE-MRI), differentiating between malignant and benign lesions and evaluating changes in response to chemoradiotherapy (CRT). Our aim was to find DCE-MRI parameters, biomarkers in evaluating the post-CRT status. Two hundred and five patients with head and neck lesions were examined with DCE-MRI sequences. The time intensity curves (TIC) were extracted and processed to acquire time-to-peak (TTP), relative maximum enhancement (RME), relative wash-out (RWO), and two new parameters attack and decay. These parameters were analyzed using univariate tests in SPSS (Statistical Package for the Social Sciences, version 17, SPSS Inc. Chicago, USA) to identify parameters that could be used to infer tumor malignancy and post-CRT changes. Multiple

parameters of curve characteristics were significantly different between malignant tumors after CRT (MACRT) and changes caused by CRT. The best-performing biomarkers were the attack and the decay. We also found multiple significant ( $p < 0.05$ ) parameters for both the benign and malignant status as well as pre- and post-CRT status. Our large cohort of data supports the increasing role of DCE-MRI in HNT differentiation, particularly for the assessment of post-CRT status along with accurate morphological imaging.

**Keywords** DCE-MRI · Head-and neck tumors · Post-treatment imaging · Chemoradiotherapy · Time intensity curve · Biomarker

## Introduction

Recent studies have shown promising results in differentiating head and neck tumors (HNT) using dynamic contrast-enhanced magnetic resonance imaging (DCE-MRI) [1, 2]. Diagnostic imaging, in addition to clinical evaluation, plays a major role in assessing the precise status of patients with HNT after chemoradiotherapy (CRT) as well as ruling out existing malignant lesions among expected post-CRT changes. However, head and neck imaging is extremely challenging, especially the post-treatment imaging after CRT. Our aim was to find DCE-MRI parameters, biomarkers to characterize head and neck lesions, with a primary focus on differentiating between expected post-CRT changes and malignant tumors after CRT. Tumor growth is closely related to angiogenesis, and DCE-MRI provides useful hemodynamic information about vascularity and vascular permeability [3]. Our hypothesis was that DCE-MRI, based on the analysis of time intensity curves (TIC), may be a helpful tool to distinguish malignant tumors after CRT from expected post-CRT changes.

✉ Gergely Lerant  
lerger@freemail.hu

<sup>1</sup> Department of Diagnostic Radiology, National Institute of Oncology, Postal Code 1122Rath Gyorgy Street 7-9, Budapest, Hungary

<sup>2</sup> Department of Measurement and Information systems, Budapest University of Technology, Budapest, Hungary

<sup>3</sup> Center of Radiotherapy, National Institute of Oncology, Budapest, Hungary

<sup>4</sup> Department of Otorhinolaryngology, Head and Neck Surgery, Semmelweis University, Budapest, Hungary

<sup>5</sup> Surgical and Molecular Tumor Pathology Centre, National Institute of Oncology, Budapest, Hungary

<sup>6</sup> Multidisciplinary Center of Head and Neck Oncology, National Institute of Oncology, Budapest, Hungary

<sup>7</sup> University of Medicine and Pharmacy of Targu Mures, Targu Mures, Romania

## Materials and Methods

A total of 205 consecutive patients (from March 2013–September 2013) with head and neck lesions included in this study. The inclusion criteria consisted of the presence of a head and neck lesion. Forty-three new malignant tumors without any prior therapy (NM), and 107 lesions classified as expected post-CRT changes without suspicion of malignancy (APCRT) were examined. Because of the inclusion criteria, some benign and inflammatory lesions were also evaluated. The APCRT group was further divided into two subgroups, the late post-CRT (LPCRT) and early post-CRT (EPCRT) groups. The LPCRT patient group was defined as stable post-CRT changes on imaging and clinical follow-up at least 12 months after CRT. Fewer than 12 months had passed since CRT for the EPCRT group, but these patients' imaging and clinical status was considered normal post-CRT changes. There were 84 patients in the LPCRT group and 23 in the EPCRT group. Sixteen malignant tumors after CRT (MACRT) were investigated, which consisted of residual/recurrent tumors after CRT. Fifteen benign tumors (BT) and 6 purely inflammatory lesions (IL) were also evaluated during the study (Table 1). Approximately ten percent of the patients ( $n=18$ ) had to be excluded from the study due to severe motion artifacts. All the tumors were histologically confirmed. In the APCRT group after CRT, a biopsy was not always performed, such biopsies were only obtained prior to the therapy. In these cases, the stable clinical and imaging follow-up data (at least 12 months after the MRI examination) confirmed that malignancy was not present. The histology of the new malignant cases and the malignant cases that received CRT were squamous cell carcinoma (SCC). The vast majority of these lesions were located in the mesopharynx ( $n=74$ ), followed by the oral cavity ( $n=32$ ), larynx ( $n=27$ ), hypopharynx ( $n=18$ ), and epipharynx ( $n=15$ ). The ILs ( $n=6$ ) were mainly located near inflamed neck cysts. The BTs were quite diverse in their histology and location, including adenomas in the thyroid ( $n=6$ ), parotid gland pleiomorphic adenomas ( $n=2$ ),

Whartin tumors ( $n=5$ ). In addition, a glomus tumor and a hemangioma located in the mesopharynx was examined.

The examinations were performed using a 3 Tesla wide-bore clinical MR scanner (General Electric Discovery 750w, Milwaukee, USA) in a single cancer institute. The imaging data were transferred to the workstation to obtain the TIC. The DCE sequence was performed as part of our routine examination, followed by fat saturated post-contrast T1 (PCT1FS) sequences in 3 planes for further diagnostic purposes. The DCE sequence was a fast spoiled gradient echo sequence (FSPGR) with 80 phases. The whole dynamic sequence took 4 min 3 s, with a 6 mm slice thickness and 3 mm overlapping slices. Overall, 14 slices centered on the lesion, which was identified on the precontrast morphologic images (1,120 slices overall). The injection procedure was standardized using a power injector. A needle was placed into an antecubital vein and, after 10 s of baseline scans, the injection was started. The injection rate was 3 ml/s with a dosage of 0.1 mmol/kg gadobenate dimeglumine (Multihance). The placement of the region of interest (ROI) was performed by two expert head and neck specialists, one having more than 20 years of experience in the field. The ROI included the entire lesion, but the obvious necrotic areas were excluded. The ROI was placed on the axial image, where the lesion showed the largest axial diameter. The conventional high-quality morphological images were used as an anatomic reference (Fig. 1).

The obtained TICs were smoothed by calculating the mean of the intensities in a sliding window 5 time slices in width. From the smoothed TICs, multiple parameters were calculated, including the time to peak (TTP), relative maximum enhancement (RME) and relative washout (RWO); the respective formulas are shown in Fig. 2. The use of these biomarkers has been promoted in recent articles [1, 2]. We also included two new biomarkers, attack and decay, which were very useful in differentiating the curves. Attack represents the area over the normalized curve (AOC) from the injection time to the maximum signal intensity ( $SI_{max}$ ), and decay represents the AOC from  $SI_{max}$  to the end time signal intensity ( $SI_{end}$ ) (Fig. 2). Both the attack and decay parameters were normalized to the area of the curve bounding box defined by ( $T_{end}$  - Inject Time)  $\times$  ( $SI_{max}$ ). We used the independent samples t-test to test for the association between the curve parameters and specific case groups. The curve parameters were analyzed using univariate tests in SPSS 17 to identify predictors that could be used to infer tumor malignancy and post-CRT status.

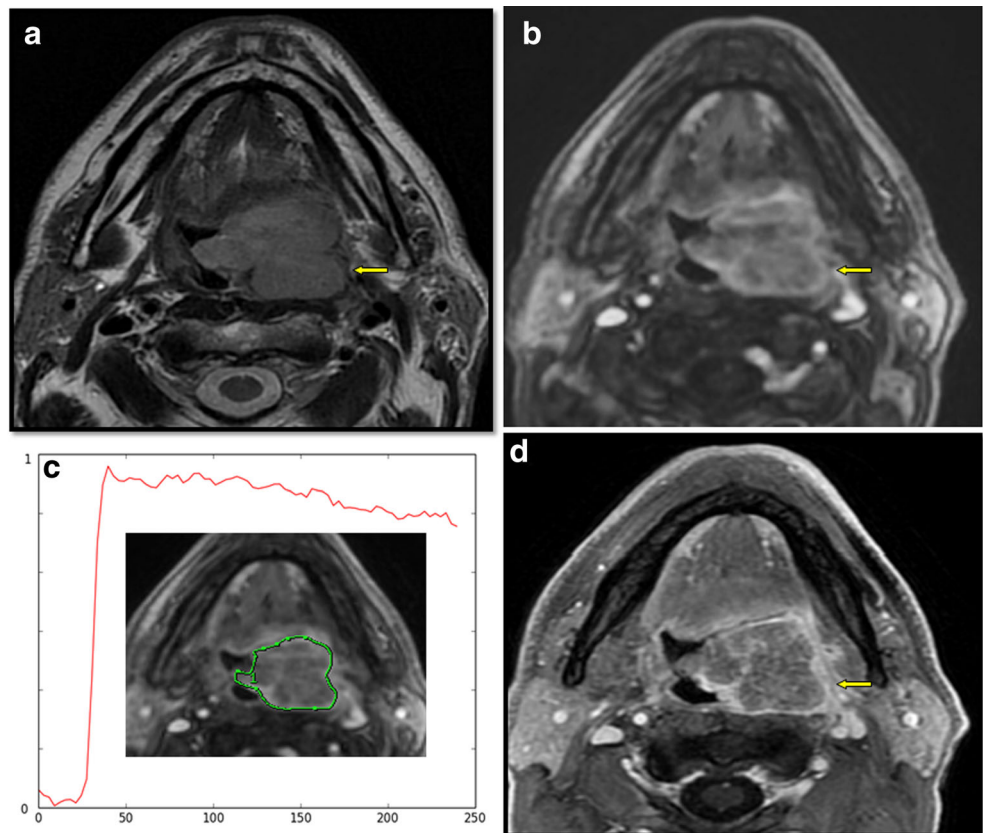
Patients were immobilized with a thermoplastic mask and treated with 3-dimensional (3D) conformal treatment or intensity-modulated radiation therapy (IMRT) using 6 MV photons. The planned radiation dose to the primary tumor and the involved lymph nodes was 70 Gy in definitive radiotherapy and chemo- or bioradiotherapy, 60–66 Gy in the case of positive surgical margin and/or extracapsular extension to the tumorbed and the involved lymph node region in the post-

**Table 1** Number of patients in each investigated groups

Number of total individual patients	205
New malignant lesion (NM)	43
Post CRT <1 years "Early" (EPCRT)	23
Post CRT >1 years "Late" (LPCRT)	84
Malignant tumor after CRT (MACRT)	16
Benign tumor (BT)	15
Inflammatory lesion (IL)	6
Excluded because of severe motion artifacts	18

NM new malignant, BT benign tumor, APCRT all post chemoradiotherapy, EPCRT early post chemoradiotherapy, LPCRT late post chemoradiotherapy, MACRT malignant after chemoradiotherapy, I inflammation

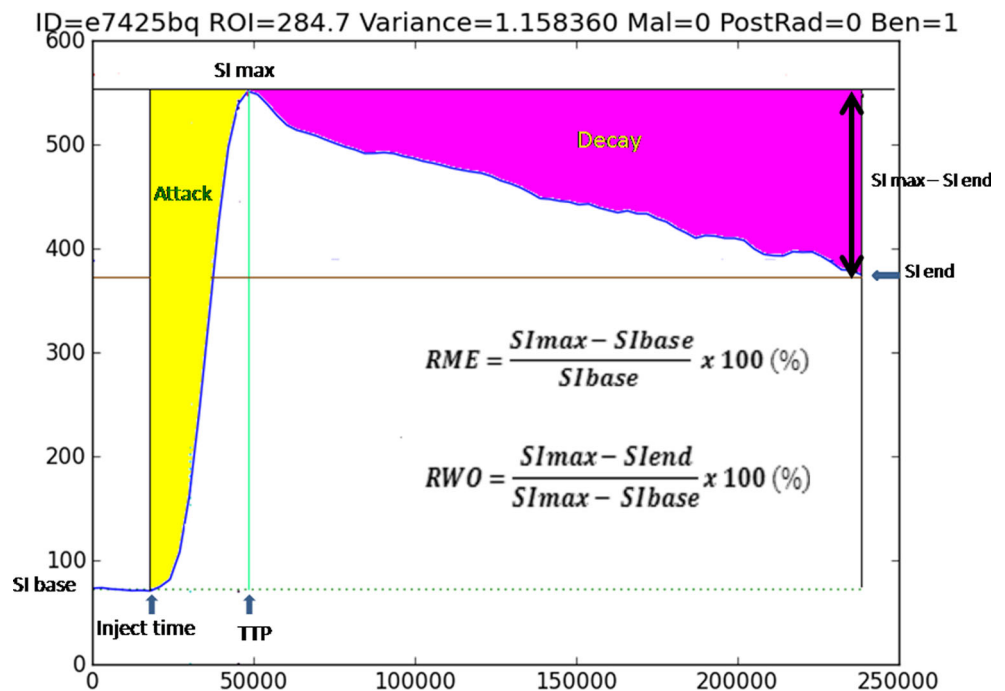
**Fig. 1** Left sided mesopharynx carcinoma, yellow arrow points to primary tumor **a**: T2 weighted precontrast image **b**: Fast spoiled gradient echo (FSPGR) dynamic image obtained under 3 s **c**: The region of interest and the corresponding time intensity curve. The X axis corresponds to the time in seconds, and the Y axis represents the normalized signal intensity **d**: Postcontrast fat saturated T1 weighted image (PCTIFS) obtained in 1 min 30 s. *FSPGR* Fast spoiled gradient echo, *PCTIFS* post contrast T1 weighted fat saturated image



operative treatment, and 50 Gy to the lymph node area of microscopic disease (2 Gy per day, 5 days per week). For chemoradiotherapy, 100 mg/m<sup>2</sup> cisplatin was administered two or three times (on the 1st, 22<sup>nd</sup> and 43<sup>rd</sup> days of

radiotherapy); for bioradiotherapy, the loading dose of cetuximab was 400 mg/m<sup>2</sup> on day 1 of the week preceding radiotherapy and, thereafter, a weekly dose of 250 mg/m<sup>2</sup> was applied during irradiation.

**Fig. 2** The investigated parameters of the time intensity curve: TTP (Time to peak), *SI*<sub>base</sub> (base signal intensity), *SI*<sub>max</sub> (maximum signal intensity), *SI*<sub>end</sub> (end signal intensity), RME (relative maximum enhancement), RWO (relative wash out), Attack and Decay. The X axis corresponds to the time in milliseconds, and the Y axis represents the signal intensity



## Patients' Rights

All procedures followed were in accordance with the ethical standards of the responsible committee on human experimentation (institutional and national) and with the Helsinki Declaration of 1975 (in its most recently amended version). Informed consent was obtained from all patients included in the study.

## Results

In our patient group, three major representative curve types were confirmed in the different groups (Fig. 3). The BTs demonstrated the fastest wash-in and wash-out pattern. The new malignant cases showed a fast wash-in section followed by a plateau pattern or a slight wash-out. The malignant tumors after CRT mostly showed almost the same curve type patterns as the newly malignant tumors, without any significant differences in our investigated parameters. The post-CRT group displayed a delayed wash-in pattern with a continuous increase in the signal intensity until the end of the measurement, and almost no wash-out was visible. ILs showed a very similar curve type as the post-CRT cases.

To compare the different investigated parameters in each comparison (e.g., NM versus BT), the independent t-test was used (Table 2).

Between the NM ( $n=43$ ) and BT ( $n=15$ ) cases, the RWO ( $p=6.2 \times 10^{-8}$ ) and decay ( $p=3.92 \times 10^{-6}$ ) were the most significantly different parameters.

Between the NM ( $n=43$ ) and APCRT ( $n=107$ ) cases, the TTP ( $p=1.8 \times 10^{-17}$ ) and attack ( $p=2.9 \times 10^{-50}$ ) were the most significantly different parameters.

Between the LPCRT ( $n=84$ ) and EPCRT ( $n=23$ ) cases, the only significant difference was observed in the RME parameter ( $p=0.045$ ).

Between the MACRT ( $n=16$ ) and EPCRT ( $n=23$ ) groups, the most significant difference was observed for the attack ( $p=5.22 \times 10^{-22}$ ) and decay ( $p=5.78 \times 10^{-6}$ ) parameters. When MACRT was compared to APCRT, the attack and decay remained the most significantly different parameters, although the significance was stronger for attack ( $p=1.22 \times 10^{-33}$ ) and decay ( $p=6.12 \times 10^{-7}$ ).

ILs ( $n=6$ ) were measured as well, and their TIC pattern was almost identical to the APCRT ( $n=107$ ), LPCRT ( $n=84$ ), and EPCRT ( $n=23$ ) groups, showing no significant difference between the investigated parameters.

Scatter plots were also created for our newly introduced parameters, showing nearly perfect separation in our groups. The MACRT and NM cases demonstrated very similar values (Fig. 4).

## Discussion

New aspects of the management of advanced HNT cases have emerged, and non-surgical therapies in the case of HNT have become standard therapy in recent years. One of the major endpoints of interest in the management of HNT is to improve the patient's quality of life and preserve organ function without compromising survival. Due to its better technical capacity, 3D-conformal IMRT has reduced the dose delivered to normal tissues because of its improved focus on the precision of target volumes. Patients with no response to standard therapy often undergo salvage surgery, although the criteria for inoperability have recently shifted, and more extended resections and reconstructions are currently performed [4–7].

As a result of these changes, more accurate assessment of tumor borders, tumor volume, and the biological target volume is needed for therapy planning. However, it remains critical to ensure that the radiological diagnosis of tumor status is concordant with the actual pathological status [5, 7]. Increased contrast enhancement after CRT is not a specific sign, and it is often very difficult to distinguish normal, expected post-CRT changes with inflammation from the pathologic neovascularization of MACRT.

Multiparametric MRI offers one of the highest possible soft tissue resolutions of imaging procedures without requiring ionizing radiation. After the complex evaluation of different MR sequences, it is possible to assess the post-therapeutic environment [8–10]. With the development of state-of-the-art MR examination techniques and sequences and the advent of high-field-strength MR scanners, the spatial and temporal resolutions have also greatly increased. These recent advances have made it possible to evaluate the distribution of the contrast agent over time, which provides information about the permeability of the tissue.

After CRT, the tumor volume shows regression, and fibrotic tissue develops. Radiation therapy is followed by an acute inflammatory reaction associated with increased permeability and interstitial edema. After several weeks, progressive thickening of the connective tissue starts to develop, leading to fibrosis [9, 10]. Purely ILs were also investigated in the current study, and these demonstrated almost the same TIC type as post-CRT changes without any significant difference in the recorded parameters. However, the IL and APCRT curves were significantly different in multiple parameters from the MACRT curves, whereas the late and early post-CRT curves showed only one significantly different parameter, RME ( $p=0.045$ ). One possible explanation for the significantly higher signal intensities observed in early post-CRT changes may be the presence of an underlying inflammatory reaction in the early stage, which later resolves. In addition, the shape of the post-CRT curves may be due to obstruction of the microvessels after irradiation [1, 11, 12]. Based on this information, the early post-CRT stage, which is the most

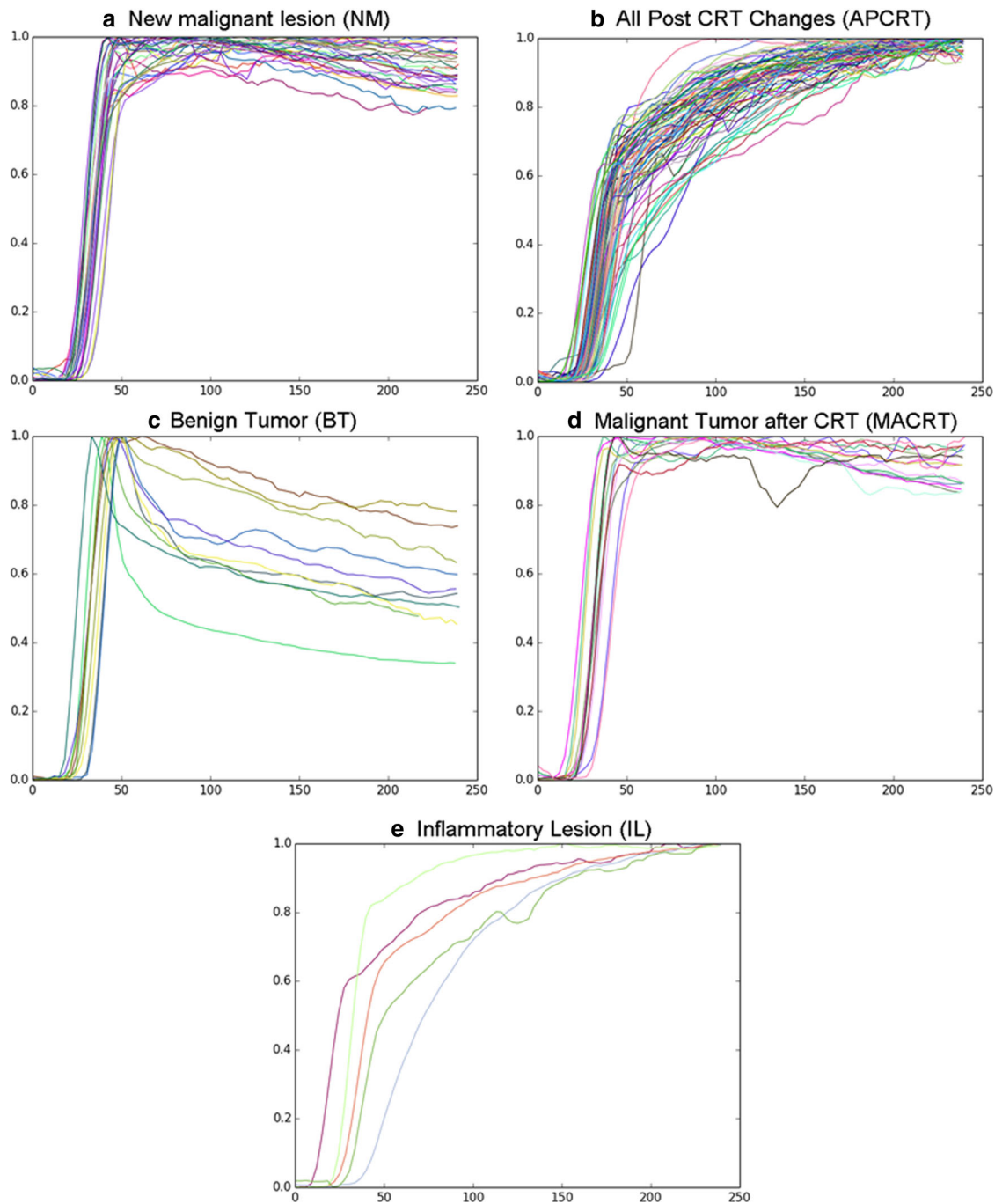


**Fig. 3** Time intensity curve types. The X axis corresponds to the time in seconds of each measurement, and the Y axis represents the normalized intensity. Each curve is colored differently to allow visual differentiation. **a:** New malignant type with fast wash in, with slow washout or plateau pattern **b:** Post chemoradiotherapy type with slow wash in with continuous rise, and late time to peak **c:** Benign type with fast wash in, fast wash out

**d:** Malignant after chemoradiotherapy with fast wash in, with slow washout or plateau pattern **e:** Inflammation type, similar to the post chemoradiotherapy type with slow wash in with continuous rise, and late time to peak. *NM* new malignant, *BT* benign tumor, *APCRT* all post chemoradiotherapy, *MACRT* malignant after chemoradiotherapy, *I* inflammation

challenging to diagnose, ILs and other expected post-CRT changes could be possible to distinguish from malignant lesions by analyzing the TIC. Baba et al. reported fast wash-in and a relatively fast wash-out in residual tumors after CRT [11, 12]. In addition, Aslihan et al. found that tumor tissue showed early and intense enhancement, which may allow to

differentiate malignancy from post-CRT changes [13], and Furukawa et al. found that TTP and RWO were the most sensitive markers in differentiating post-CRT changes and MACRT [1]. In our study, the newly introduced parameters, biomarkers attack and decay, performed better (with lower p values), although TTP and RWO also showed significant

**Table 2** P values Colors yellow: non-significant ( $p < 0,05$ ), orange: significant ( $0,01 < p < 0,05$ ), green: highly significant ( $p < 0,01$ )

	NM vs BT	NM vs APCRT	NM vs EPCRT	NM vs MACRT	MACRT vs EPCRT	MACRT vs APCRT	EPCRT vs LPCRT	IL vs APCRT	IL vs EPCRT
TTP	$2.2 \times 10^{-5}$	$1.8 \times 10^{-17}$	$3.2 \times 10^{-14}$	0.922	$1.6 \times 10^{-5}$	$7.9 \times 10^{-7}$	0.06	0.503	0.857
RME	$6.2 \times 10^{-3}$	0.86	0.02	0.72	0.68	0.048	0.045	0.910	0.273
RWO	$6.2 \times 10^{-8}$	$1.3 \times 10^{-10}$	$2.7 \times 10^{-8}$	0.228	$1.1 \times 10^{-5}$	$1.3 \times 10^{-6}$	0.228	0.261	0.131
Attack	$2.5 \times 10^{-5}$	$2.9 \times 10^{-50}$	$1.1 \times 10^{-14}$	0.631	$5.2 \times 10^{-22}$	$1.2 \times 10^{-33}$	0.685	0.853	0.915
Decay	$3.9 \times 10^{-6}$	$4.9 \times 10^{-9}$	$7.3 \times 10^{-7}$	0.42	$5.8 \times 10^{-6}$	$6.1 \times 10^{-7}$	0.245	0.883	0.534

NM new malignant, BT benign tumor, APCRT all post chemoradiotherapy, EPCRT early post chemoradiotherapy, LPCRT late post chemoradiotherapy, MACRT malignant after chemoradiotherapy, I inflammation

differences, which is in agreement with other recent findings. In addition, most of the NM and MACRT curves were very similar and showed no significant difference in any of the investigated parameters. Rashed L. et al. found that malignant tumors after irradiation mainly showed early enhancement with plateau pattern, or rapid enhancement followed by a slight washout [14]. This is the same curve patterns we found in this group. In some MACRT curves we did see longer TTP than in NM which we assume the effect of irradiation but upon comparison it did not reach statistical significance. Beside the early enhancement pattern with plateau or with slight washout, we also found two EPCRT cases where later malignancy appeared, but this two cases had gradual enhancement pattern which caused some overlap with the clinically negative cases. Prior studies [1, 11, 12] have assumed that the leakiness of the blood vessels in malignant tumors could explain the shape of the NM and MACRT curves. Two cases were included to show the possible use of TIC analyses in the post-CRT environment, and to present the different curve types. (Fig. 5)

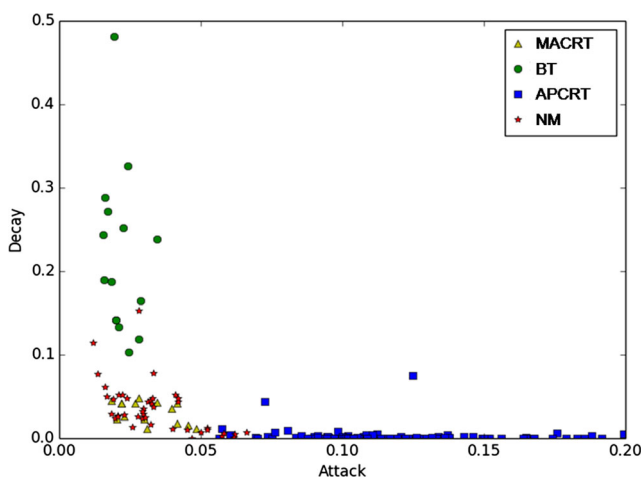


**Fig. 4** Scatter plot showing the respective attack and decay values for each case type. Yellow triangles represent malignant tumors after CRT (MACRT), green circles show benign tumors (BT), blue squares are all post CRT changes (APCRT) and red stars are new malignant tumors (NM). MACRT malignant tumors after chemoradiotherapy, NM new malignant, BT benign tumor, APCRT all post chemoradiotherapy

Since our study ended, the vast majority ( $n=19$ ) of the patients in the early post-CRT group (mean time 3, 6 months, range 3–11 months after CRT), who were considered at the time of examination to have normal post-CRT changes clinically (based on physical examination, and on imaging with the supportive role of TIC analyses), have been still showing normal post-CRT status without any clinical or imaging evidence of malignancy. Although in 2 patients we only have 6 months of proper follow up and in 2 cases having a gradual enhancement TIC pattern, after 3 and 6 months of follow up respectively, malignancy appeared. A possible explanation to their curve pattern is that if the surrounding inflammation is large and compared to that the tumor size is smaller, because the signal intensities in the ROI is averaged in our study, the mean curve will be very close to the inflammation/post CRT types. Pixel by pixel analysis, and color coding the entire neck area with the use of parameters like Attack and Decay may overcome this drawbacks. But even with this overlaps these findings may demonstrate the value of TIC analyses in the EPCRT group.

Because of the inclusion criteria of this study, some cases, which were later histologically proven to be BTs, were also investigated. In our study, the TIC curves of the BTs were significantly different in multiple parameters from the NM as well as post-CRT curves. The benign cases demonstrated significantly faster wash-out than the new malignant cases, and the most significantly different parameters between these groups were the RWO and decay. There were some overlap here too, this is mainly due to the pleomorphic adenomas, which according to the literature can have gradual enhancement pattern (6), or as in our study they are very close to the malignant type curves [15]. The main limitation for BTs in our study is the relatively low number of them ( $n=15$ ) and that the histology and location of benign lesions were quite diverse. Sumi et al. concluded that besides analysis of the TIC, the intravoxel incoherent motion diffusion-weighted imaging (IVIM-DWI) technique could also be very useful, especially when these two methods are combined [16].

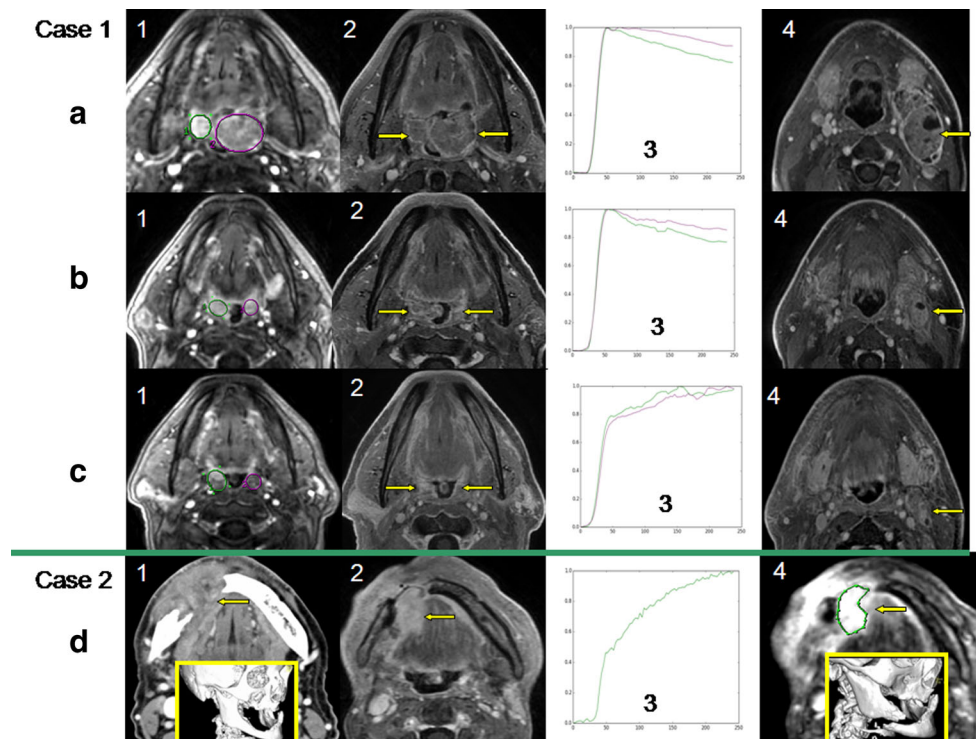


**Fig. 5** **a** Row Case 1 bilateral tonsillar tumor before treatment: dynamic sequence, ROI on both tumor sites (A1), Corresponding PCT1FS, yellow arrows point to tumors (A2) malignant type TIC curves, the color of the curve refers to the ROI color (A3) PCT1FS pathologic neck nodes, yellow arrow points to the largest node (A4) **b** Row Case 1 bilateral tonsillar tumor 3 months follow up after treatment: dynamic sequence, ROI on both decreasing tumor sites (B1), Corresponding PCT1FS, yellow arrows point to decreasing tumors (B2) malignant/MACRT type TIC curves, the color of the curve refers to the ROI color (B3) PCT1FS pathologic neck nodes, yellow arrow points to the decreasing node (B4) **c** Row Case 1 bilateral tonsillar tumor 6 months follow up after treatment: dynamic sequence, ROI on both prior tumor sites (C1), corresponding PCT1FS, yellow arrows point to prior tumor sites (C2) post CRT/inflammation type TIC curves, the color of the curve refers to the ROI color (C3) PCT1FS pathologic neck nodes, yellow arrow points decreasing node (C4) Because of the persisting pathologic nodes surgery was performed with bilateral tonsillectomy, and at the former

tumor site only fibrosis was present with minimal surrounding inflammation. **d** Row Case 2 Enhancing lesion at the right sided large gingival tumor site after CRT Original tumor site, axial contrast enhanced computer tomography (CE-CT), and 3 dimensional CT reconstruction, note the mandibular destruction (D1) 10 months after treatment near a pathologic mandibular fracture: dynamic sequence, ROI on the enhancing lesion and 3D CT reconstruction, note the surrounding enhancement which is also inflammation (D4) post CRT/inflammation type TIC curve (D3) Corresponding PCT1FS, with the well circumscribed still enhancing lesion that was included in the ROI (D2). Mandibular resection was performed, the histology was only inflammation with no sign of malignancy. *CRT* chemoradiotherapy, *ROI*: region of interest, *PCT1FS* post contrast T1 weighted fat saturated image, *MACRT* malignant tumors after chemoradiotherapy, *CRT* chemoradiotherapy, *TIC* time intensity curve, *CE-CT* contrast enhanced computer tomography, *3D CT reconstruction*: 3 dimensional computer tomography reconstruction

The variance of the curves was mostly related to the presence of motion artifacts, which is the biggest drawback of using this method. Motion artifact severity or variance is derived from the sum of the difference of the normalized and smoothed normalized curves. The appearance of motion artifacts significantly correlated with the localization ( $p=0.02$ ) of the region. The most severe motion artifacts were present in the region of the larynx and hypopharynx (mean variance over 2), and the lowest variance (mean variance below 1) was observed in the epipharynx.

The role of PET/CT in the assessment of post-treatment status has become more standardized, and there are new promising results from PET/MR [17–21]. CT perfusion of the head and neck has also shown some promising results in assessing the status of the head and neck area [22]. Although CT is more

widely available and costs less, radiation exposure limits its applicability.

As part of the most up-to-date multiparametric imaging, diffusion-weighted imaging DWI has shown very promising results in the recent literature on differentiating malignant lesions from post-treatment changes [23–27].

New directions in the field of DCE-MRI are experimenting with pixel by pixel analyses and color-coding of the entire head and neck area using DCE-MRI [28], and one study reported differentiating undifferentiated carcinoma from squamous cell carcinoma or from lymphoma using DCE-MRI [29].

This study also has its limitations. Our patient number is high but the vast majority of the cases are new malignant and stable LPCRT cases ( $N=127$ ) which with the correct clinical information are rarely a question on morphologic imaging. To

further analyze the role of DCE MRI in the early post-treatment patient groups, additional prospective studies with a larger sample size of EPCRT cases and residual/recurrent tumors from different centers are needed, and pixel by pixel analysis with color coding using parameters like our newly described Attack and Decay may overcome the overlaps. Due to the consecutive nature of the study the time of examination after CRT were also quite varied and in case of stable post CRT status biopsy was mainly not taken. In our study, the MACRT lesions were relatively large and quite well delineated, as Hungary has a very high prevalence and mortality of head and neck cancers, and these patients often have very advanced T3-T4 stage tumors. However, if the persisting tumor after CRT is small and the surrounding inflammation and post-CRT changes are much larger, it could be very difficult to outline and distinguish malignancy from CRT changes, even with high-quality multiparametric imaging. Heterogeneity of the tumor enhancement and necrotic areas could also be very challenging, and these factors could result in mixed curve types, as the signal intensities of the ROI in our study were averaged.

Even with these limitations, TIC analyses of DCE-MRI adds another promising tool to the analysis of post-treatment lesions. Integrating DCE-MRI sequence into normal diagnostic workflow is relatively easy, whereas it is not time consuming. Obtaining and analyzing the TIC has a relatively short learning curve, but because of the complex anatomy, pathology and imaging of the head and neck area, experience is required to define the ROI, especially in the early posttreatment status. With respect to cost, it is not expensive because these patients, unless there are contraindications, already receive a contrast agent. Moreover, diagnostic post-contrast high resolution T1 images could be acquired after the dynamic sequences, which have remained the main stay of head and neck diagnostic imaging.

## Conclusion

Based on our larger cohort of data, DCE-MRI has potential in analyzing the post CRT environment. This method represents a useful part of high-quality multiparametric MRI, although severe motion artifacts (which are not uncommon in patients with HNT, especially after treatment) could hamper the efficiency of this method. The main value of the TIC analyses of DCE-MRI is supportive information with the aid of high-quality morphological imaging, and it might be used to determine post-therapeutic changes as well as to evaluate differences between diagnostic modalities.

**Acknowledgments** This study was supported by the National Institute of Oncology

**Conflicts of Interest** Gergely Lerant states that there are no conflicts of interest

Peter Sarkozy states that there are no conflicts of interest

Zoltan Takacs-Nagy states that there are no conflicts of interest

Gabor Polony states that there are no conflicts of interest

Laszlo Tamas states that there are no conflicts of interest

Erika Toth states that there are no conflicts of interest

Andras Boer states that there are no conflicts of interest

Laszlo Javor states that there are no conflicts of interest

Maria Godeny states that there are no conflicts of interest

## References

1. Furukawa M, Parvathaneni U, Maravilla K, Richards TL, Anzai Y (2013) Dynamic contrast-enhanced MR perfusion imaging of head and neck tumors at 3 Tesla. *Head Neck* 35:923–929
2. Yuan Y, Yue XH, Tao XF (2012) The diagnostic value of dynamic contrast-enhanced MRI for thyroid tumors. *Eur J Radiol* 81:3313–3318
3. Kim S, Loevner LA, Quon H, Kilger A, Sherman E, Weinstein G, Chalian A, Poptani H (2010) Prediction of response to chemoradiation therapy in squamous cell carcinomas of the head and neck using dynamic contrast-enhanced MR imaging. *AJNR Am J Neuroradiol* 31:262–268
4. Gődény M (2014) Prognostic factors in advanced pharyngeal and oral cavity cancer; significance of multimodality imaging in terms of 7th edition of TNM. *Cancer Imaging* 14:1–13
5. Grégoire V, Lefebvre J, Licitra L, Felip E (2010) Squamous cell carcinoma of the head and neck: EHSN-ESMO-ESTRO clinical practice guidelines for diagnosis, treatment and follow-up. *Ann Oncol* 21(5):v184–v186
6. Hermans R, De Keyzer F, Vandecaveye V, Carp L (2012) *Head and neck cancer imaging*. Springer, Berlin/Heidelberg, Germany
7. Licitra L, Felip E, ESMO Guidelines Working Group (2009) Squamous cell carcinoma of the head and neck: ESMO clinical recommendations for diagnosis, treatment and follow-up. *Ann Oncol* 20:iv121–iv122
8. Hermans R (2006) Head and neck cancer: how imaging predicts treatment outcome. *Cancer Imaging* 6:S145–S153
9. Hermans R (2008) Posttreatment imaging in head and neck cancer. *Eur J Radiol* 66:501–511
10. Saito N, Nadgir RN, Nakahira M, Takahashi M, Uchino A, Kimura F, Truong MT, Sakai O (2012) Posttreatment CT and MR imaging in head and neck cancer: what the radiologist needs to know. *Radiographics* 32:1261–1282
11. Baba Y, Furusawa M, Murakami R, Yokoyama T, Sakamoto Y, Nishimura R, Yamashita Y, Takahashi M, Ishikawa T (1997) Role of dynamic MRI in the evaluation of head and neck cancers treated with radiation therapy. *Int J Radiat Oncol Biol Phys* 37:783–787
12. Baba Y, Yamashita Y, Onomichi M (2002) Dynamic MR imaging and radiotherapy. *Magn Reson Med Sci* 1:32–37
13. Semiz Oysu A, Ayanoglu E, Kodalli N, Oysu C, Uneri C, Erzen C (2005) Dynamic contrast-enhanced MRI in the differentiation of posttreatment fibrosis from recurrent carcinoma of the head and neck. *Clin Imaging* 29:307–312
14. Rashed L et al. (2010) The added value of DWI MRI in characterization of tissue in treated head and neck tumors. *Egypt J Ear Nose Throat* 11
15. Chikui T et al. (2012) The principal of dynamic contrast enhanced MRI, the method of pharmacokinetic analysis, and its application in the head and neck region *Int J Dent* Article ID 480659 <http://dx.doi.org/10.1155/2012/480659>

16. Sumi M, Nakamura T (2014) Head and neck tumours: combined MRI assessment based on IVIM and TIC analyses for the differentiation of tumors of different histological types. *Eur Radiol* 24:223–231
17. Andrade RS, Heron DE, Degirmenci B, Filho PA, Branstetter BF, Seethala RR, Ferris RL, Avril N (2006) Posttreatment assessment of response using FDG-PET/CT for patients treated with definitive radiation therapy for head and neck cancers. *Int J Radiat Oncol Biol Phys* 65:1315–1322
18. Dunsky KA, Wehrmann DJ, Osman MM, Thornberry BM, Varvares MA (2013) PET-CT and the detection of the asymptomatic recurrence or second primary lesions in the treated head and neck cancer patient. *Laryngoscope* 123:2161–2164
19. Escott EJ (2013) Role of positron emission tomography/computed tomography (PET/CT) in head and neck cancer. *Radiol Clin N Am* 51:881–893
20. Tantiwongkosi B, Yu F, Kanard A, Miller FR (2014) Role of (18)F-FDGPET/CT in pre and post treatment evaluation in head and neck carcinoma. *World J Radiol* 6:177–191
21. Queiroz MA, Hüllner M, Kuhn F, Huber G, Meerwein C, Kollias S, von Schulthess G, Veit-Haibach P (2014) PET/MRI and PET/CT in follow-up of head and neck cancer patients. *Eur J Nucl Med Mol Imaging* 41:1066–1075
22. Romboldt Z, Al-Okaili R, Deveikis JP (2005) Perfusion CT for head and neck tumors: pilot study. *AJNR Am J Neuroradiol* 26:1178–1185
23. Vandecaveye V, de Keyzer F, Vander Poorten V, Deraedt K, Alaerts H, Landuyt W, Nuyts S, Hermans R (2006) Evaluation of the larynx for tumour recurrence by diffusion-weighted MRI after radiotherapy: initial experience in four cases. *Br J Radiol* 79:681–687
24. Vandecaveye V, De Keyzer F, Nuyts S, Deraedt K, Dirix P, Hamaekers P, Vander Poorten V, Delaere P, Hermans R (2007) Detection of head and neck squamous cell carcinoma with diffusion weighted MRI after (chemo) radiotherapy: correlation between radiologic and histopathologic findings. *Int J Radiat Oncol Biol Phys* 67:960–971
25. Vandecaveye V, De Keyzer F, Dirix P, Lambrecht M, Nuyts S, Hermans R (2010) Applications of diffusion-weighted magnetic resonance imaging in head and neck squamous cell carcinoma. *Neuroradiology* 52:773–784
26. Vandecaveye V, Dirix P, de Keyzer F, de Beeck KO, Vander Poorten V, Roebben I, Nuyts S, Hermans R (2010) Predictive value of diffusion-weighted magnetic resonance imaging during chemoradiotherapy for head and neck squamous cell carcinoma. *Eur Radiol* 20:1703–1715
27. Vandecaveye V, Dirix P, De Keyzer F, de Op Beeck K, Vander Poorten V, Hauben E, Lambrecht M, Nuyts S, Hermans R (2012) Diffusion-weighted magnetic resonance imaging early after chemoradiotherapy to monitor treatment response in head-and-neck squamous cell carcinoma. *Int J Radiat Oncol Biol Phys* 82:1098–1107
28. Yuan J, Chow SK, Yeung DK, King AD (2012) A five-colour colour-coded mapping method for DCE-MRI analysis of head and neck tumours. *Clin Radiol* 67:216–223
29. Lee FK, King AD, Ma BB, Yeung DK (2012) Dynamic contrast enhancement magnetic resonance imaging (DCE-MRI) for differential diagnosis in head and neck cancers. *Eur J Radiol* 81:784–788